Intensity Statistics-based HSI Diffusion for Color Photo Denoising

Lei He
Information Technology Dept.
Armstrong Atlantic State University
Savannah, GA 31419
Lei.He@armstrong.edu

Chunming Li
Inst. of Imaging Science
Vanderbilt University
Nashville, TN 37232
Chunming.Li@vanderbilt.edu

Chenyang Xu
Imaging & Visualization Dept.
Siemens Corporate Research
Princeton, NJ 08540
Chenyang.Xu@siemens.com

Abstract

This paper presents a new image denoising model for real color photo noise removal. Our model is implemented in the hue, saturation and intensity (HSI) space. The hue and saturation denoising are combined and implemented as a complex total variation (TV) diffusion. The intensity denoising is based on a diffusion flow to minimize a new energy functional, which is constructed with intensity component statistics. Besides the common gradient-based edge stopping functions for anisotropic diffusion, specifically for color photo denoising, we incorporate an intensity-based brightness adjusting term in the new energy, which corresponds to the noise disturbance with respect to photo intensity. In addition, we use the gradient vector flow (GVF) as the new diffusion directions for more accurate and robust denoising. Compared with previous diffusion flows only based on regular image gradients, this model provides more accurate image structure and intensity noise characterization for better denoising. Comprehensive quantitative and qualitative experiments on color photos demonstrate the improved performance of the proposed model when compared with 14 recognized approaches and 2 commercial software.

1. Introduction

In the past two decades, image denoising has been a fundamental and active research topic and widely used as a key step in a variety of image processing and computer vision applications, such as image segmentation, compression, object recognition and tracking. Since the seminal work proposed by Perona and Malik [1] in the early 1990s, numerous literatures have been presented to recover the "true" image from noisy data through anisotropic diffusions [2-16,20,24-28], robust statistics [17,25], as well as transformation-based approaches (e.g. wavelet [15,20], ridgelet and curvelet-based image denoising [21]), just to name a few. A complete review of current image denoising approaches can be seen in several recent literatures [19,22].

With the widespread usage of digital cameras, color photo noise removal has become an important research subject. Noise in color photo is introduced in the process of image acquisition, filtering, compression and reconstruction. In digital photography, a high ISO setting of a digital camera is usually used to increase light sensitivity in dark environments, but the resultant image contains more sensor noise than a low ISO image taken with the same exposure[1]. The objective of our work is to denoise high ISO photos to achieve a low ISO photo quality without the use of expensive cameras or accessories. The motivation comes from the practical needs of digital camera users and manufacturers [30]. So far, most existing approaches are used to solve a general denoising problem (e.g. gray, color or multi-spectral images) based on an assumption of additive or multiplicative noise independent of signal and to the best of our knowledge, none of presented literatures focus on the unknown digital camera sensor noise in color photos.

This paper presents a novel framework for color photo denoising, particularly those photos taken at a high ISO setting that resulted in noticeable sensor noise. Compared with existing literatures, there are two major contributions in this paper. The first is that our approach implements color photo denoising in the HSI (hue, saturation and intensity) space instead of the traditional RGB (red, green and blue) space because the HSI model has a better color description for human interpretation [18]. Particularly, the intensity component denoising is our main focus, which is implemented by a diffusion flow derived from a new energy functional minimization. Besides using edge stopping terms to characterize major image structure, we specifically incorporate a brightness adjusting term in the energy to approximate the noise disturbance with respect to color photo intensity. All these terms are constructed directly from the intensity component statistics. In addition, we use the gradient vector flow (GVF) [23] directions to guide the diffusion for more accurate and robust denoising. The derived diffusion flow extends common gradient-based anisotropic diffusions to a model based on both GVF directional derivatives and intensity, which provides more accurate image structure and intensity noise characterization for better denoising. The

[1] This is achieved by reducing the shutter speed or increasing the aperture.

978-1-4244-2243-2/08/$25.00 ©2008 IEEE

hue and saturation components are combined as a complex image and diffused in the traditional total variation (TV) [9] form. The second contribution is the algorithm performance assessment. In most existing literatures, artificial noise (e.g. Gaussian noise) has been employed for algorithm performance evaluation. Furthermore, the denoising effect has been assessed mostly by human visual perception, few by the mean squared error (MSE) and the peak signal to noise ratio (PSNR). In contrast, the color photo noise produced by digital cameras is real sensor noise. In this paper, the proposed algorithm is evaluated by comparing the denoised photos with ground truth[2]. The ground truth and noisy photos are produced by the same camera on the same scene with low and high ISO settings by maintaining the same exposure. We perform a comprehensive performance comparison of our proposed algorithm, current recognized methods and commercial software using objective error measurements (the PSNR and MSE) and the commonly used subjective visual assessment. Both quantitative and qualitative validation shows that the proposed algorithm is more appropriate for color photo denoising than existing approaches.

2. Background

One major category of image denoising approach is implemented via anisotropic diffusion flows, either implemented directly in the form of partial differential equations (PDE) [1-7,24], or derived from certain optimization problems using variational methods [8-16,20,25-28]. For direct PDE-based approaches, given an image I: $\Omega \subset \Re^2 \to \Re^m$, a continuous sequence of smoother images I_t are generated by $I_t = R(I)$, with $R(I)$ representing an image regularization term. For anisotropic diffusion, this term restricts the smoothing in two principles: 1) the magnitude of smoothing, e.g. less smoothing at edges; 2) the direction of smoothing, e.g. less smoothing in the directions across edges. For example, a diffusion equation using a general form of $R(I)$ is

$$I_t = R(I) = g(|\nabla I|)I_{\eta\eta} + h(|\nabla I|)I_{\xi\xi}, \qquad (1)$$

where $g(\cdot)$ and $h(\cdot)$ are gradient-based weighting functions (called "diffusivity" or "edge stopping" functions) to control the smoothing amount along the η (normal) and ξ (tangential) directions. Various functions of $g(\cdot)$ and $h(\cdot)$ [1-5] and diffusion directions [6,7] have been proposed for accurate noise removal and image feature preservation. In a recent paper [24], GVF is applied to replace the high-order derivative terms in several popular models, including the Perona-Malik equation [1], shock filter [5] and the mean curvature flow [4]. In this paper, specifically for color photo denoising, we extend the anisotropic diffusion principles by incorporating a new intensity-based term with gradient-based terms in the diffusion flow, i.e., less smoothing not only at edges, but also at intensities with small noise.

Variational methods usually formulate image denoising as an optimization problem with an objective function, and the optimum produces the "noise-free" image. Numerous objective functions have been proposed for optimization, such as the image total variation [9,10,26], hypersurface areas [11,12,27], Mumford-Shah functional and its variations [13,14], and the a posteriori probability in Bayesian equation [15,16,20,25]. TV-based methods are typically presented as a minimization of the image total variation ($\int |\nabla I| d\Omega$) with certain constraints. In [11,12,27], an image is modeled as an embedding manifold (harmonic mapping) that flows (Beltrami flow) toward the minimal surface in a higher dimensional space (hypersurface). When a priori knowledge of image structure is known, the denoising problem can be formulated as a maximum a posteriori probability (MAP) estimation [15,16,20,25]. Note that variational methods in fact are closely related to the direct PDE diffusions. By variational principle, the optimization process is usually implemented by PDEs [3,22].

The techniques introduced above however do not explicitly account for the noise statistics in the diffusion flows. In [17], image noise statistics is embedded into the diffusion PDEs through different $g(\cdot)$ and $h(\cdot)$ functions. Without using iterative PDE-based diffusions, a non-local mean algorithm [19] applies image redundancy for denoising, i.e., a pixel value is replaced by a weighted intensity summation of its neighbors. Image statistics has also been used in the MAP methods [16,25] to construct the image prior models.

While most existing color image denoising methods are implemented in the RGB space, few in other color spaces, e.g. the chromaticity and brightness (CB) space [8,26], the hue, saturation and value (HSV) space [26-28]. These spaces are used because they are considered to be closer to human visual perception [26]. In these methods, chromaticity or hue denoising are usually the main focus. The models in [8,26-28] are extensions of the TV [9] and Beltrami flow [11] to the CB and HSV spaces. In this paper, we denoise color photos in the HSI space and the intensity component denoising is our main focus, which is implemented by minimizing a new statistics-based energy functional. The hue and saturation denoising are combined and implemented as a complex TV diffusion [26]. With a set of low and high ISO color photos, we also conduct a comprehensive performance comparison between our algorithm and 14 recognized approaches for different color spaces (the CB [8,26], HSV [26,27] and RGB spaces [1,2,3,4,5,10,12,13,17,19]), and 2 commercial color photo denoising software (Noiseware™ [29] and Photoshop™).

[2] All the photos and denoising results in this paper can be obtained from the author's website: http://cs.armstrong.edu/leihe/Project_Denoising.htm.

3. Proposed approach

3.1. Intensity diffusion

In the HSI space, the intensity component, denoted by I, of a color image is the average of the red, green and blue values, which corresponds to the gray version of the color image. Thus it transfers the most important information for human visual "feeling" on the image. In our approach, the color photo intensity component diffusion is implemented by a variational method. As described in Section 2, variational methods usually solve image denoising problem by minimizing a certain energy functional. A common form of such energy is

$$E(I) = \int_{\Omega} \left(\psi(|\nabla I|) + \frac{\lambda}{2}(I - I_0)^2 \right) d\Omega , \qquad (2)$$

where I_0 is the original image, $\psi(\cdot)$ is a univariate function, and $\lambda>0$ is a constant. In Eq. (2), $\psi(|\nabla I|)$ and $(I-I_0)^2$ are the diffusion term and data term respectively. Practically, the diffusion term is usually defined as a function of image gradient [3,22] for edge preservation in diffusion. The data term is to prevent the diffusion result deviating too much from the original image I_0.

With only gradient-based diffusion term, Eq. (2) does not address noise effects directly based on image intensities. In this paper, specifically for color photo denoising, we construct a new energy functional consisting of not only gradient-based terms to characterize image structure (i.e., for edge preserving), but also an intensity-based term to measure the noise disturbance on photo intensity (i.e., for brightness adjusting). Furthermore, we introduce new diffusion directions (GVF directions [23]) by replacing the regular image gradient with GVF-based directional derivatives. Therefore, our energy functional is defined as

$$E(I) = \int_{\Omega} \left(\sum_{j=1}^{2} \psi_j(I, |\mathbf{n}_j^T \nabla I|) + \frac{\lambda}{2}(I - I_0)^2 \right) d\Omega , \quad (3)$$

where $\psi_j(\cdot)$ are new diffusion terms based on both intensity and directional derivatives, and $\mathbf{n}_j$ refers to different derivative directions. Different from the common η-ξ directions used in most approaches, the GVF direction, $\mathbf{v}(\mathbf{x}) = (u(\mathbf{x}), v(\mathbf{x}))^T$, $\mathbf{x} \in \Re^2$, is applied in our algorithm for more accurate denoising, i.e., the diffusion directions are $(\mathbf{n}_1, \mathbf{n}_2)$ with $\mathbf{n}_1 \parallel \mathbf{v}$ and $\mathbf{n}_2 \perp \mathbf{v}$. The GVF was initially proposed for image segmentation with desirable properties, e.g. its regularity and capability of denoising the gradients and closing small gaps in boundaries, which are more beneficial than regular image gradient for edge identification and preservation in image denoising. Note that the GVF is used in our method with the same objective for more stable and accurate denoising as the GVF-based diffusions in [24], but we use a different framework with a new energy functional more targeted for color photo denoising.

Figure 1(b) and 1(c) compare the gradient and GVF fields of a synthetic image in Figure 1(a), in which the scattered dark dots are added as image noise and the blur part at the square top is a weak boundary. It can be seen that the GVF field is preferable to the gradient field for its more regular diffusion directions with all the vectors pointing to the correct edges. Using the same diffusivity [22] and diffusion PDE (Eq. (1)), but different diffusion directions, (η, ξ) and $(\mathbf{n}_1, \mathbf{n}_2)$, we can obtain the diffusion results based on the gradient field and GVF in Figure 1(d) and 1(e). With comparable iteration numbers, the GVF-based diffusion accurately removes all noise points and preserves the weak boundary, while the gradient-based diffusion over smoothes the weak boundary and fails on some noise points even after a long iteration.

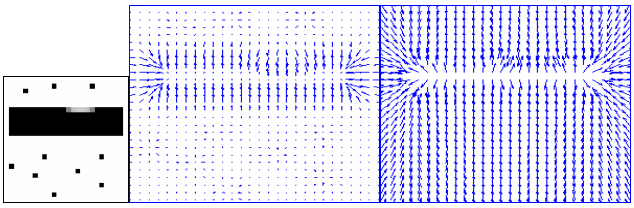

(a) A test image **(b)** The gradient field of **(a)** **(c)** The GVF field of **(a)**

(d) Gradient-based diffusion results at 10 and 100 iterations **(e)** GVF-based diffusion results at 10 and 100 iterations

Figure 1: Comparison of diffusion results based on image gradient and GVF

In our approach, we construct the diffusion term with independent intensity- and derivative-based terms, i.e.,

$$\psi_j(I, |\mathbf{n}_j^T \nabla I|) = \varphi(I)\varphi_j(|\mathbf{n}_j^T \nabla I|) , \qquad (4)$$

where $\varphi(I)$ and $\varphi_j(|\mathbf{n}_j^T \nabla I|)$ are the proposed *brightness adjusting term* (BAT) and *edge stopping term* (EST) in the diffusion equation. Different from most existing approaches, these terms are all derived from the intensity component spatial statistics. As indicated earlier, the BAT is a measure of the noise disturbance on color photo intensity. It is specifically included here for intensity-based adaptive smoothing, i.e., less smoothing at intensities with small noise. This is motivated by researches on digital camera sensor noise [31]. With a pair

of low and high ISO photos, we can obtain the BAT by measuring the difference ("error") of the photos at different intensity values. For example, Figure 2 illustrates three low ISO photos[3] and their corresponding BAT statistics after normalization. In our application, we use a simple curve to simulate this intensity noise disturbance,

$$\varphi(I)=\begin{cases}\varepsilon I & 0\le I<c_1\\ \varepsilon(I-c_2) & 255\ge I>c_2\\ 1-\dfrac{1}{1+\exp(-(I-L_I)C_I/255)} & \text{otherwise}\end{cases}, \qquad (5)$$

where c_1 and c_2 are lower and upper intensity threshold values, $0<\varepsilon<<1$, L_I and C_I are translation and scaling factors. If both low and high ISO photos are available, the curve parameters can be obtained by curve fitting[4]. For the EST, a variety of gradient-based functions [22] have been proposed for adaptive smoothing (e.g. less smoothing at edges). Here we use the functions directly based on the directional derivative distributions as in [25], which is a Student-t distribution, i.e., $p(x)=\frac{1}{N}(1+\frac{x^2}{\sigma^2})^{-t}$, where N is a normalization factor, $t>0$ and σ are scale parameters to make the $p(x)$ proper distributions. As in [25], we obtain

$$\varphi_j(|\mathbf{n}_j^T\nabla I|)=-\log(\frac{1}{N_j}(1+\frac{|\mathbf{n}_j^T\nabla I|^2}{\sigma_j^2})^{-t}). \qquad (6)$$

Similar to the BAT, we can obtain the parameters in Eq. (6) by curve fitting. Due to the space limit, Figure 2 only illustrates the directional derivative distributions and EST curve fitting results for the first example. Similar results can be obtained for the other two examples.

Therefore, by calculus of variations, we can obtain the diffusion PDE of Eq. (3) as:

$$\frac{\partial I}{\partial t}=\mathbf{div}\left(\varphi(I)\sum_j\frac{\varphi_j'(|\mathbf{n}_j^T\nabla I|)}{|\mathbf{n}_j^T\nabla I|}\mathbf{n}_j\mathbf{n}_j^T\nabla I\right)-\varphi'(I)\sum_j\varphi_j(|\mathbf{n}_j^T\nabla I|)-\lambda(I-I_0). \qquad (7)$$

[3] In this paper, the low (ISO=100) and high ISO (ISO=1600) photos (size=300×300) presented for quantitative comparison were cut separately from big pictures (3456×2304 or 3888×2592) taken at the same scene with different ISO settings.

[4] For example, we use Matlab's fminsearch function for curve fitting.

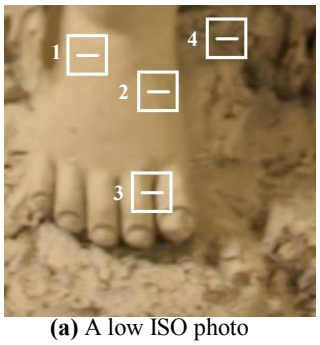

(a) A low ISO photo

(b) The high ISO photo of **(a)**

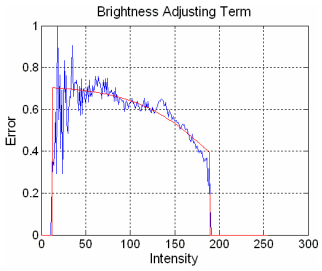

(c) Noise disturbance with respect to photo intensity of **(a)** and BAT curve fitting by Eq. (5)

(d) The denoising result of **(b)** with the proposed approach

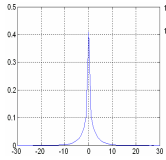

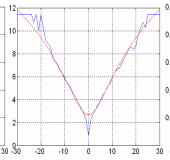

(e) $\mathbf{n}_1^T\nabla I$ distribution of **(b)** and EST curve fitting by Eq. (6)

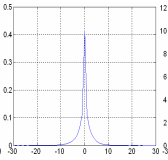

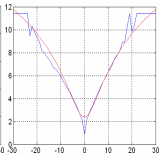

(f) $\mathbf{n}_2^T\nabla I$ distribution of **(b)** and EST curve fitting by Eq. (6)

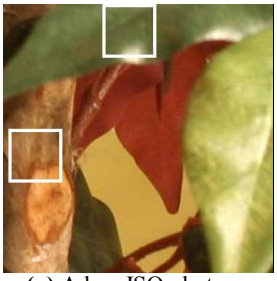

(g) A low ISO photo

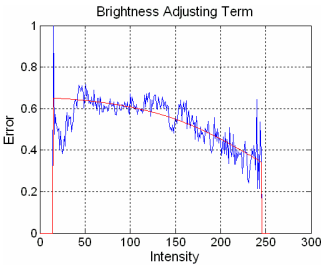

(h) BAT curve fitting of **(g)**

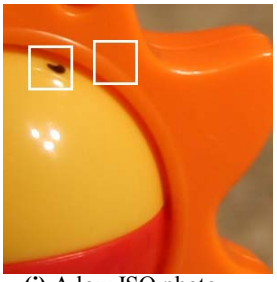

(i) A low ISO photo

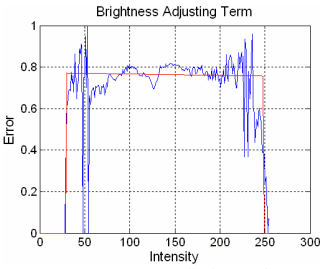

(j) BAT curve fitting of **(i)**

Figure 2: BAT: $\varphi(I)$ and EST: $\varphi_j(|\mathbf{n}_j^T\nabla I|)$ in Eq. (4). Red curves are fitting results with Eqs. (5) and (6) for BAT and EST statistics.

3.2. Hue and saturation diffusion

In the HSI space, the hue component (H) is an attribute to describe a pure color and is measured as an angle. The saturation component (S) gives a measure of the degree to which a pure color is diluted by white light and is represented as a distance map. Due to the periodicity of angles, the direct extension from intensity diffusion to hue would cause ambiguity. Similar to the HSV diffusion in [26], we combine the hue and saturation components to be a complex number: $Z = S\exp(2\pi H\mathrm{i})$, and diffuse Z in the traditional TV framework

$$\frac{\partial Z}{\partial t} = \mathrm{div}\left(\frac{\nabla Z}{|\nabla Z|}\right) - \eta(Z - Z_0), \qquad (8)$$

$\eta>0$, $Z_0 = S_0\exp(2\pi H_0\mathrm{i})$ is the original input. To avoid a zero denominator in numerical implementation, a small constant $\alpha>0$ is added in $|\nabla Z|$ as $|\nabla Z|_\alpha = \sqrt{|\nabla Z|^2 + \alpha}$. Eq. (8) can be decoupled to two PDEs for the real (R) and imaginary (M) components (i.e., $Z = R + M\mathrm{i}$)

$$\begin{cases} \dfrac{\partial R}{\partial t} = \dfrac{\begin{pmatrix} R_{xx}(\alpha + R_y^2 + |\nabla M|^2) - R_x(R_y R_{xy} + M_x M_{xx} + M_y M_{xy}) + \\ R_{yy}(\alpha + R_x^2 + |\nabla M|^2) - R_y(R_x R_{xy} + M_x M_{xy} + M_y M_{yy}) \end{pmatrix}}{(\alpha + |\nabla R|^2 + |\nabla M|^2)^{3/2}} \\ \qquad -\eta(R - R_0) \\ \dfrac{\partial M}{\partial t} = \dfrac{\begin{pmatrix} M_{xx}(\alpha + M_y^2 + |\nabla R|^2) - M_x(R_x R_{xx} + R_y R_{xy} + M_y M_{xy}) + \\ M_{yy}(\alpha + M_x^2 + |\nabla R|^2) - M_y(R_x R_{xy} + R_x R_{yy} + M_x M_{xy}) \end{pmatrix}}{(\alpha + |\nabla R|^2 + |\nabla M|^2)^{3/2}} \\ \qquad -\eta(M - M_0) \end{cases}$$

The interested reader is referred to [26] for more details of this complex diffusion.

4. Experiments

Two experiments have been conducted on color photos taken by four digital cameras. For the first, two sets of ten color photos have been collected by a Canon 350D and a 400D on the same indoor scenes with different ISO settings. The low and high ISO photos of one scene are used as the ground truth and the noise corrupted version. The indoor photos are obtained with a carefully calibrated setup to maintain the consistence of lighting between two photo captures. The photo scene contains only static objects to avoid any motion blur. Only shutter speed is adjusted to maintain the same exposure. Aperture is kept fixed to preserve the same depth of field in both low and high ISO photos. As introduced earlier, with the ground truth available, we compare our HSI BAT-based approach (BAT) with 14 recognized methods in the CB [8,26], HSV [26,27] and RGB [1,2,3,4,5,10,12,13,17,19] color spaces, and 2 commercial software (Noiseware™ [29] and Photoshop™), using both quantitative (the PSNR and MSE) and qualitative (visual perception) measures. Due to the space limit, here we only present four approaches with the highest ranked performance from the quantitative comparison, i.e., the modified curvature flow [12], vector diffusion [3], non-local mean algorithm [19] and CB TV [26], as well as a popular color photo denoising software (Noiseware™). In the second experiment, a qualitative comparison is performed by 10 people on a set of outdoor photos taken by a Sony CyberShot P72 and a S650, which demonstrates the generality of our approach.

4.1. Quantitative comparison experiment

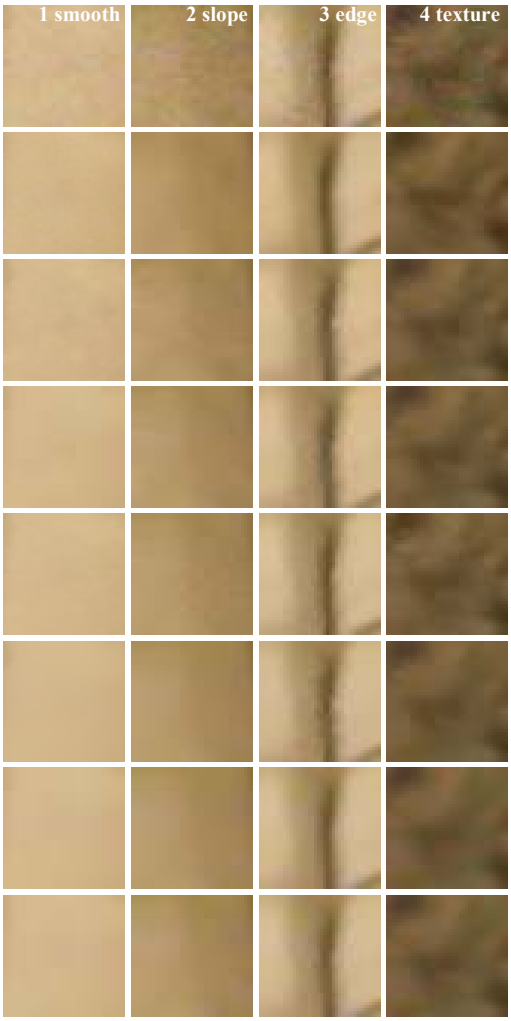

Figure 3: Denoising results sorted by the PSNR and MSE

Using the first example in Figure 2, Figure 3 shows the denoising results of the selected approaches on different image features (e.g. smooth region, slope, edge and texture). For a clear view, we only display four enlarged regions (see Figure 2(a)) in the high and low ISO photos (Figure 3(a),3(b)) and the denoising results. The results of

Figure 3(c)-3(h) are sorted by the optimal PSNR and MSE values for visual comparison. Due to the close PSNR (MSE) values, these results look similar on the whole. Though, as the error increases, it can be seen some small features are smoothed away from the truth (e.g. at the right region 4). To test more varied images, we repeated this comparison on other nine photo pairs (including Figure 2 examples). Figure 6 compares the average quantitative error of these ten results.

In order to highlight the behavior of the proposed BAT algorithm on different image features, we draw four lines (see Figure 2(a)) in the intensity components of denoising results and compare the values on these lines with the ground truth pixel by pixel. Figure 4 demonstrates the intensity errors along the lines. For a clear view, we only compare four images of Figure 3(a), 3(c), 3(d) and 3(e) with the ground truth of Figure 3(b), instead of all the results in Figure 3. The results of CB TV and Noiseware™ (Figure 3(d),3(e)) are included in this comparison because they are quantitatively ranked the second and third best. It can be seen that the proposed BAT diffusion in overall performs better than other approaches on image feature preservation and noise removal, i.e., closer to the ground truth (low ISO photo).

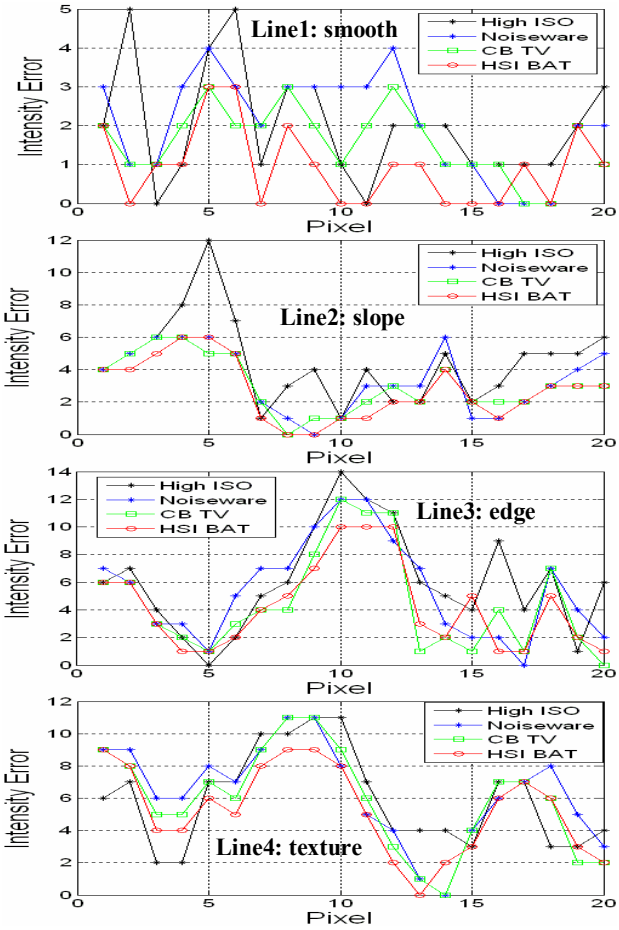

Figure 4: Denoising results line intensity comparison

We repeat this comparison on other nine pairs of photos of different scenes, including Figure 2 examples. For the other two examples in Figure 2, two selected regions with different features in the photos are shown in Figure 5(c)-5(h) and 5(k)-5(p), with the results being sorted by the optimal PSNR and MSE values. Similar to Figure 3, these approaches produce visually similar results. Though, as shown in the enlarged regions, some fine details can be preserved only by the BAT diffusion and Noiseware™, e.g. the details in the circles in the results. The mean and standard deviation of the PSNR and MSE are computed on these ten denoised photos (including Figure 3 and Figure 5 results). Figure 6 shows the chart sorting the mean values of the PSNR and MSE, with the high ISO values listed as a reference. The numbers above the bars are the corresponding mean values of the PSNR and MSE. The standard deviation values are marked as the vertical lines on the bars. It can be seen that even with the simple BAT curve fitting (see Figure 2(c), 2(h) and 2(j)), our approach outperforms other methods with the quantitative measures in average, which shows the robustness of the proposed BAT approach.

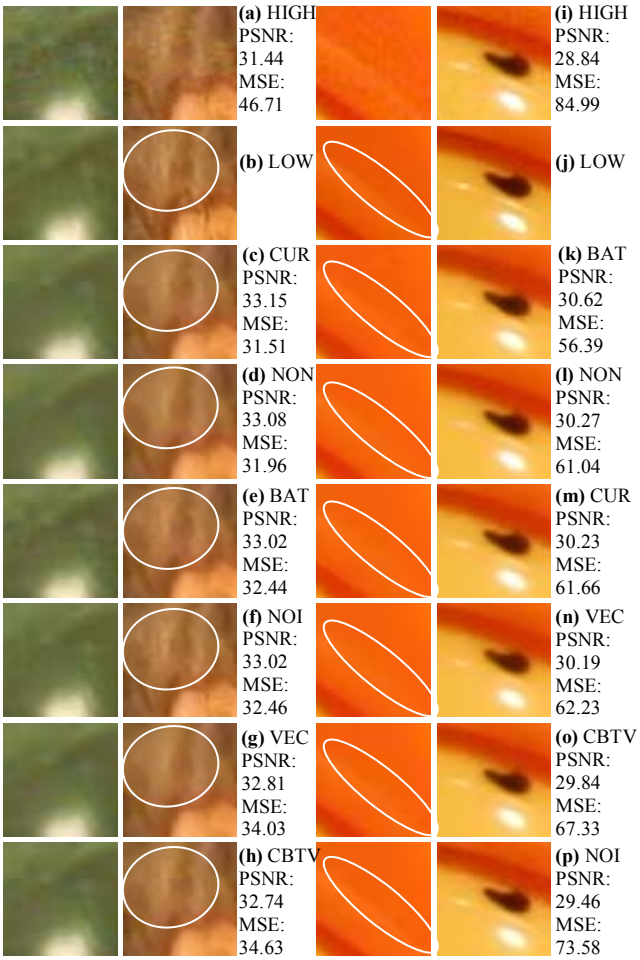

Figure 5: Denoising results sorted by the PSNR and MSE

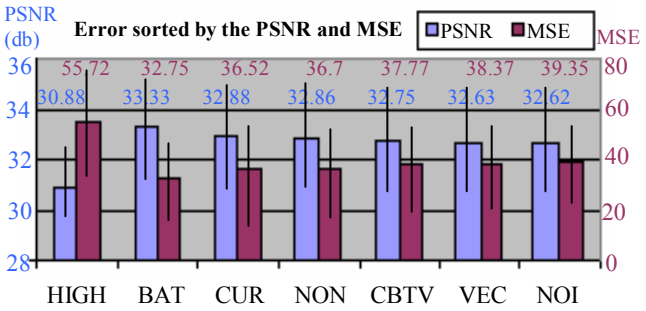

Figure 6: Error chart sorted by the average of PSNR and MSE of ten denoising results

4.2. Qualitative comparison experiment

The second experiment is conducted on a set of outdoor photos taken by a Sony CyberShot P72 and a S650 with different camera settings. Because the environmental light changes continually, there is no ground truth for these photos. The BAT and EST curve parameters are manually tuned. Figure 7 illustrates five examples (size 300×300) cut from the original photos (size 2048×1536 and 3072×2048) and the corresponding denoising results of the proposed BAT approach[5]. The results of selected approaches have been blindly evaluated by 10 people. The rankings are from the best (#1) to the worst (#6) and different methods may have the same ranking values. Table 1 shows the percentage of people with the top two rankings (#1 and #2) on the results. For example, 80% people ranked the BAT approach #1 or #2 for the result in Figure 7(a). It can be seen that the mean ranking values approximately match the quantitative comparison results in the first experiment (Figure 6) except that Noiseware™ has a much better visual ranking than its quantitative performance. With these examples, our algorithm visually outperforms other approaches in average.

Image	BAT	CUR	NON	CBTV	VEC	NOI
(a)	80%	40%	70%	20%	10%	0%
(b)	60%	20%	40%	20%	20%	80%
(c)	60%	40%	20%	0%	0%	80%
(d)	60%	60%	50%	30%	30%	70%
(e)	60%	40%	30%	10%	0%	70%
Mean **(a)—(e)**	64%	40%	43%	16%	12%	60%

Table 1: Qualitative rankings of the outdoor photo denoising results in **Figure 7**. A percentage score represents the percentage of the people ranking the corresponding result among the best two performers.

[5] Due to the space limit, we only present the proposed BAT approach results. The denoising results of other approaches can be obtained from the author's website.

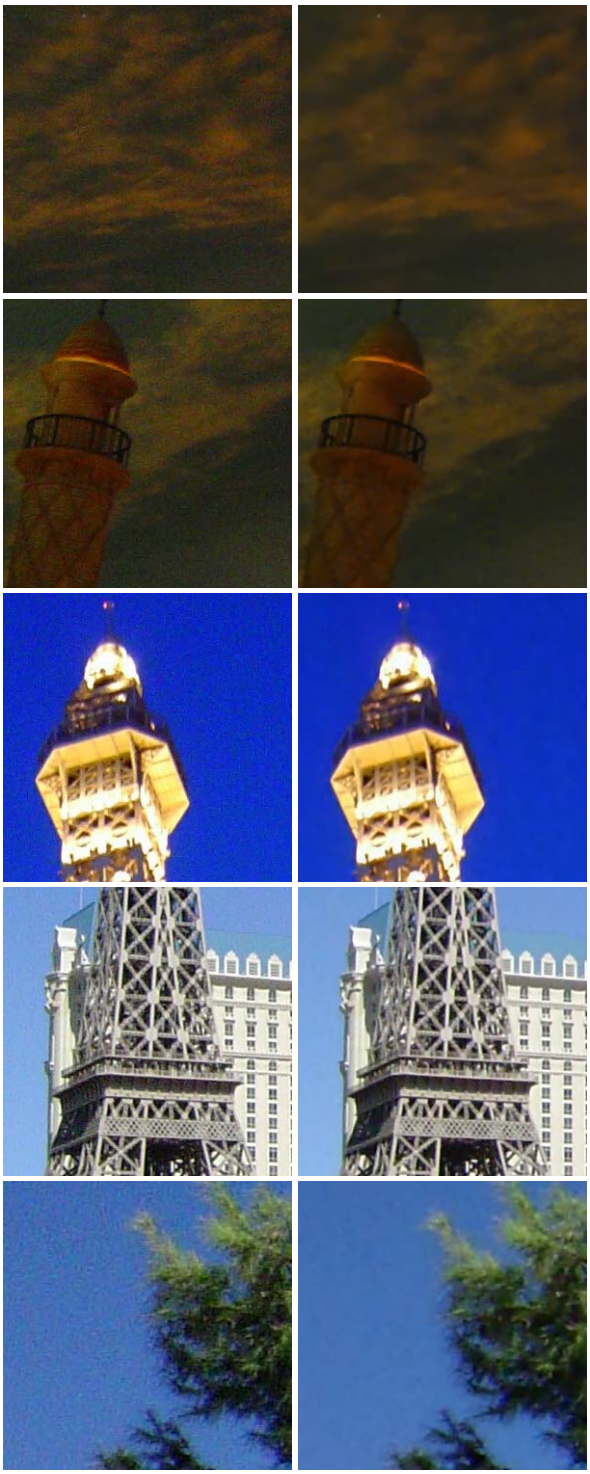

Figure 7: The proposed BAT approach denoising results of outdoor photos, left: outdoor photos, right: denoising results, top to bottom: **(a)** — **(e)**.

5. Summary

We present a novel color photo denoising method in the HSI space. The objective is to remove high ISO photo

noise to obtain a low ISO photo quality. Our main contribution is the derivation of a new energy functional for intensity component denoising. We incorporate an intensity-based brightness adjusting term (BAT) with traditional gradient-based edge stopping terms in the new energy functional. Both terms are constructed with the photo intensity statistics. The BAT is proposed to describe the noise disturbance with respect to the photo intensity. Thus the new diffusion flow implements adaptive smoothing based on both intensity and gradient, i.e., less smoothing at small noise and edges. In addition, we replace the regular gradient field with the image GVF as the new diffusion directions for more accurate and robust denoising. The hue and saturation denoising are combined and implemented as a complex TV diffusion. The performance of the proposed algorithm has been assessed quantitatively and qualitatively in the experimental comparison with 14 recognized approaches and 2 commercial software. The results indicate that the proposed approach accomplishes our goal and is competitive with the current state of the art. For future works, we will make efforts to collect ground truth for outdoor photos to further evaluate our algorithm performance. We will also investigate the techniques to automatically derive the BAT curves for photos without ground truth. Furthermore, the proposed BAT diffusion can be extended to other image modalities such as multi-spectral medical and remote sensing images.

References

[1] P. Perona, J. Malik. Scale-space and edge detection using anisotropic diffusion. IEEE TPAMI, 12(7):629-639, 1990.

[2] G. Gilboa, N. Sochen, and Y. Zeevi. Image enhancement and denoising by complex diffusion processes. IEEE TPAMI, 26(8):1020-1036, 2004.

[3] D. Tschumperle, R. Deriche. Vector-valued image regularization with PDEs: a common framework for different applications. IEEE TPAMI, 27(4):506-517, 2005.

[4] R. Malladi, J.A. Sethian. Image processing: flows under min/max curvature and mean curvature. Graphical Models and Image Processing, 58(2):127–141, 1996.

[5] L. Alvarez, L. Mazorra. Signal and image restoration using shock filters and anisotropic diffusion. SIAM J. Numerical Anal., 31(2):590-605, 1994.

[6] R. Carmona, S. Zhong. Adaptive smoothing respecting feature directions. IEEE TIP, 7(3):353–358, 1998.

[7] J. Weickert. Coherence-enhancing diffusion filtering. IJCV, 31(2/3):111–127, 1999.

[8] B. Tang, G. Sapiro, and V. Caselles. Color image enhancement via chromaticity diffusion. IEEE TIP, 10(5):701–707, 2001.

[9] L. Rudin, S. Osher, and E. Fatemi. Nonlinear total variation based noise removal algorithms. Physica D, 60:259-268, 1992.

[10] P. Blomgren, T.F. Chan. Color TV: total variation methods for restoration of vector-valued images. IEEE TIP, 7(3):304–309, 1998.

[11] N. Sochen, R. Kimmel, and R. Malladi. A general framework for low level vision. IEEE TIP, 7(3):310-318, 1998.

[12] A. Yezzi. Modified curvature motion for image smoothing and enhancement. IEEE TIP, 7(3):345-352, 1998.

[13] J. Shah. A common framework for curve evolution, segmentation and anisotropic diffusion. In Proc. IEEE CVPR, pp.136-142, 1996.

[14] A. Tsai, A. Yezzi, and A. Willsky. Curve evolution implementation of the Mumford–Shah functional for image segmentation, denoising, interpolation, and magnification. IEEE TIP, 10(8):1169-1186, 2001.

[15] J. Portilla, V. Strela, M.J. Wainwright, and E.P. Simoncelli. Image denoising using scale mixtures of Gaussian in the wavelet domain. IEEE TIP, 12(11):1338–1351, 2003.

[16] S. Roth, M.J. Black. Fields of experts: a framework for learning image priors. In Proc. IEEE CVPR, pp.860-867, 2005.

[17] M. Black, G. Sapiro, D. Marimont, and D. Heeger. Robust anisotropic diffusion. IEEE TIP, 7(3):421-432, 1998.

[18] R.C. Gonzalez, R.E. Woods. Digital Image Processing. 3rd Ed. Pearson Prentice Hall, 2008.

[19] A. Buades, B. Coll, and J.M. Morel. A review of image denoising algorithms, with a new one. Multiscale Modeling and Simulation, 4(2):490-530, 2005.

[20] M. Malfait, D. Roose. Wavelet-based image denoising using a Markov random field a priori model. IEEE TIP, 6(4):549–565, 1997.

[21] J.L. Starck, E.J. Candès, and D.L. Donoho. The curvelet transform for image denoising. IEEE TIP, 11(6):670–684, 2002.

[22] J. Weickert. Anisotropic Diffusion in Image Processing. Teubner-Verlag, 1998.

[23] C. Xu, J.L. Prince. Snakes, shapes, and gradient vector flow. IEEE TIP, 7(3):359–369, 1998.

[24] H. Yu, C. Chua. GVF-based anisotropic diffusion models. IEEE TIP, 15(6):1517–1524, 2006.

[25] H. Scharr, M. Black, and H. Haussecker. Image statistics and anisotropic diffusion. In Proc. IEEE ICCV, pp.840-847, 2003.

[26] T. Chan, S.H. Kang, and J. Shen. Total variation denoising and enhancement of color images based on the CB and HSV color models. J. of Visual Communication and Image Representation, 12:422-435, 2001.

[27] R. Kimmel, N. Sochen. Orientation diffusion or how to comb a porcupine. J. of Visual Communication and Image Representation, 13:238-248, 2002.

[28] N. Sochen, C. Sagiv, R. Kimmel. Stereographic combing a porcupine or studies on direction diffusion in image processing. SIAM J. Applied Math., 64(5):1477-1508,2004.

[29] Noiseware™, http://www.imagenomic.com/products.aspx.

[30] Professional Photographer Magazine, http://www.ppmag.com/bonus/2006/08/review-imagenomic-noiseware.html.

[31] Clark Vision: Digital Camera Sensor Analysis, http://www.clarkvision.com/imagedetail/index.html#sensor_analysis.